PERGAMON

International Journal of Solids and Structures 39 (2002) 3451–3467

INTERNATIONAL JOURNAL OF SOLIDS and STRUCTURES

www.elsevier.com/locate/ijsolstr

Striping of nematic elastomers

Eliot Fried *, Vladimir Korchagin

Department of Theoretical and Applied Mechanics, University of Illinois, Urbana-Champaign, Urbana, IL 61801-2935, USA

Received 13 February 2002

Abstract

We consider a recent experiment of Kundler and Finkelmann (Macromol. Rapid Commun. 16 (1995) 679), who subjected an aligned specimen of nematic elastomer to uniaxial extension and observed the formation of striped domains. In so doing, we apply the general theory for nematic elastomers developed by Anderson et al. (J. Elast. 56 (1999) 33) and work with an energy density that combines the effects included in the molecular-statistical theory of nematic rubber elasticity with the Oseen–Zöcher–Frank theory of nematic curvature elasticity. Assuming that the deformation and orientation fields remain in-plane, we arrive at a boundary-value problem which admits solutions corresponding to striped states. We use elementary aspects of bifurcation theory to explore the local stability of these solutions. We also obtain analytical estimates for the energy and thickness of interstripe domain walls as functions of imposed extension and compare these with numerical predictions.

Keywords: Nematic elastomers; Stripe formation; Bifurcation; Stability

1. Introduction

A *nematic elastomer* is a rubber-like solid formed by the cross-linking of a polymeric fluid which includes liquid-crystalline molecules as elements of its main chain and/or as pendant side groups. Like nematic liquid crystals, these materials possess local orientational order but lack the long-range translational order of crystalline solids.

Here, we focus on the analysis of an experiment performed by Kundler and Finkelmann (1995). The specimens used in this experiment were prepared by a two-step cross-linking reaction. Liquid-crystalline mesogens and the two cross-linking components were added to poly[oxy(methylsilylene)] in a solution of toluene. In the first reaction step, a weakly cross-linked network was formed. After removing the solvent, a uniaxial nematic phase was formed. The network was then subjected to an external mechanical stress and

* Corresponding author. Fax: +1-217-244-5707.
E-mail address: e-fried@staff.uiuc.edu (E. Fried).

0020-7683/02/$ - see front matter
PII: S0020-7683(02)00169-5

additional cross-links were formed, resulting in a uniaxial nematic elastomer with known step-length anisotropy. The specimens used in the experiment were very thin rectangular sheets with in-plane lengths of 100 mm along the axis of the load and 70 mm perpendicular to the axis of the load. To study the interaction between loading and nematic orientation, these specimens were cut at various angles to the nematic axis. We focus on the case where the specimens were cut with the nematic axis in-plane and perpendicular to the axis of the load. In this situation, Kundler and Finkelmann (1995) found that the transparent monodomain present in the uniaxially aligned nematic state breaks up into an opaque polydomain structure with striped domains realigning clockwise and counterclockwise towards the axis of the load. While gross simple shear is suppressed by the clamps on the specimen, it appears that simple shear is present in each striped domain. Kundler and Finkelmann (1995) observed the existence of strain threshold of ~ 1.1 below which reorientation does not occur and measured a characteristic stripe width of ~ 15 μm. Subsequent to the work of Kundler and Finkelmann (1995), Roberts et al. (1997) observed that when stretch is applied perpendicular to the nematic axis of an acrylate-based nematic elastomer the orientation switches discontinuously, without evidence of localized inhomogeneities or domain formation. In the wake of this controversy, Talroze et al. (1999) and Zubarev et al. (1999) conducted an exhaustive series of experiments with an acrylate-based elastomer and found that, depending on the geometrical aspect ratio of the specimen, both scenarios are possible. Specifically, when the sample is long in the direction of loading, the scenario of a homogeneous orientation switch is realized, whereas when the sample is short, the scenario of a striped pattern formation is realized.

In the present paper, we apply the general theory for nematic elastomers developed by Anderson et al. (1999) but work with a particular expression for the energy density. This expression combines the effects of the neo-Hookean theory of nematic rubber elasticity with the Oseen–Zöcher–Frank theory of nematic curvature elasticity. We assume that the deformation is a plane strain involving a uniform stretch along the axis of loading, a uniform contraction along the axis of referential orientation, and a shear within the plane defined by these two axes. Further, we assume that, during the process of stretching and reorientation, the nematic orientation remains within the plane defined by the axes of loading and referential orientation. Our formulation leads to a boundary-value problem for the shear and director angle. We find that inhomogeneous solutions to this boundary-value problem correspond to striped states. Using bifurcation theory, we study the local stability of inhomogeneous solutions. We also obtain analytical estimates for the thickness and energy of an interstripe layer. These estimates show that the thickness of a layer is independent of the number of stripes present in the specimen but that the energy of a layer varies depends on the number of stripes present. This variation occurs because the amplitude of the angle that describes the orientation field depends upon the number of stripes present. We also use numerical methods to solve the boundary-value problem. For physically relevant choices of the material parameters, we compute solutions to the boundary-value problem and use these solutions to determine the thickness and energy of a single interstripe layer. Despite the approximate nature of our analytical estimates, we find that these compare favorably with the numerical results.

Previously, the problem of striping in a nematic elastomer has been considered by Verwey et al. (1996) and Fridrikh and Terentjev (1999). These works differ from ours in two main features. First, and most importantly, Verwey et al. (1996) and Fridrikh and Terentjev (1999) use an energy density that includes a gradient term which is not properly invariant under superposed rigid changes of observer. Here, we require that the energy density be properly invariant. As an interesting consequence of this requirement, we find that the thickness of an interstripe layer depends upon the axial extension of the specimen. A second difference is that Verwey et al. (1996) and Fridrikh and Terentjev (1999) rely on a variational description of equilibrium. Here, we work directly with the equations of equilibrium. Hence, while the solution of our problem involves the determination of a pressure field necessary to ensure the constraint of incompressibility, this consideration is completely absent from the analysis of Verwey et al. (1996) and Fridrikh and Terentjev (1999).

2. Preliminaries

We consider an incompressible nematic-elastomeric body that, in a reference state, occupies a region $\mathscr{R}$ in a three-dimensional Euclidean point space $\mathscr{E}$. To describe the macroscopic kinematics, we introduce a deformation $\boldsymbol{y}$ which assigns to each point $\boldsymbol{x}$ of $\mathscr{R}$ a point $\boldsymbol{y}(\boldsymbol{x})$ of $\mathscr{E}$. We write $\boldsymbol{F} = \operatorname{grad}\boldsymbol{y}$ for the deformation gradient and, due to the incompressibility of the medium, require that $\det \boldsymbol{F} = 1$. To describe the microstructural kinematics, we introduce a step length $\boldsymbol{L}$ which assigns to each point $\boldsymbol{x}$ in $\mathscr{R}$ a symmetric and positive-definite tensor $\boldsymbol{L}(\boldsymbol{x})$ that describes any nematically induced distortion of the polymer chains.

3. Constitutive assumptions

The molecular-statistical theory of Warner et al. (1988) yields an expression,

$$\psi_{\text{bulk}} = \frac{\mu}{2}\left(\operatorname{tr}\left(\boldsymbol{L}^{-1/2}\boldsymbol{F}\boldsymbol{L}_0\boldsymbol{F}^{\top}\boldsymbol{L}^{-1/2}\right) + \log\det(\boldsymbol{L}^{-1}\boldsymbol{L}_0) - 3\right), \tag{3.1}$$

for the bulk energy density of an incompressible nematic elastomer in terms of $\boldsymbol{F}$ and $\boldsymbol{L}$. Appearing in (3.1) are two material parameters—the step length $\boldsymbol{L}_0$ in the reference state and the shear modulus $\mu > 0$. Like $\boldsymbol{L}$, $\boldsymbol{L}_0$ takes only symmetric and positive-definite values.

In the specimens used by Kundler and Finkelmann (1995), $\boldsymbol{L}_0$ has the uniaxial form

$$\boldsymbol{L}_0 = \ell_{\perp}\boldsymbol{1} + (\ell_{\parallel} - \ell_{\perp})\boldsymbol{n}_0 \otimes \boldsymbol{n}_0, \tag{3.2}$$

where $\boldsymbol{n}_0$, with $|\boldsymbol{n}_0| = 1$, determines the nematic orientation in the undeformed reference state and $\ell_{\perp} > 0$ and $\ell_{\parallel} > 0$ are the molecular step-lengths perpendicular and parallel to the orientation. Motivated by the experimental observations, we restrict attention to situations where, in the deformed state, the medium remains uniaxial and the molecular step-lengths are unaltered; then, $\boldsymbol{L}$ has the form

$$\boldsymbol{L} = \ell_{\perp}\boldsymbol{1} + (\ell_{\parallel} - \ell_{\perp})\boldsymbol{n} \otimes \boldsymbol{n}, \tag{3.3}$$

where $\boldsymbol{n}$, with $|\boldsymbol{n}| = 1$, determines the nematic orientation in the deformed state.

In view of (3.2) and (3.3), we introduce the step-length anisotropy

$$s = \frac{\ell_{\parallel}}{\ell_{\perp}} > 0 \tag{3.4}$$

and, employing (3.2)–(3.4), expand (3.1) to give

$$\psi_{\text{bulk}} = \frac{\mu}{2}\left(|\boldsymbol{F}|^2 - \frac{s-1}{s}|\boldsymbol{F}^{\top}\boldsymbol{n}|^2 + (s-1)|\boldsymbol{F}\boldsymbol{n}_0|^2 - \frac{(s-1)^2}{s}(\boldsymbol{F}^{\top}\boldsymbol{n}\cdot\boldsymbol{n}_0)^2 - 3\right). \tag{3.5}$$

The energy density (3.5) describes the material response in regions in which $\boldsymbol{n}$ is homogeneous—as may be the case within individual stripes. To account for variations of $\boldsymbol{n}$ that occur across transition layers separating stripes, we introduce a gradient-energy density

$$\psi_{\text{grad}} = \frac{\kappa(s-1)^2}{2s}|\boldsymbol{F}^{\top}\boldsymbol{G}|^2, \tag{3.6}$$

with $\boldsymbol{G} = \operatorname{grad}\boldsymbol{n}$. This expression arises on setting $k_1 = k_2 = k_3 = \kappa(s-1)^2/2s$ and $k_4 = 0$ in the generalization [1]

$$\begin{aligned}&\tfrac{1}{2}(k_1 - k_2 - k_4)(\boldsymbol{F}\cdot\boldsymbol{G})^2 + \tfrac{1}{2}(k_3 - k_2 - k_4)|\operatorname{sym}(\boldsymbol{F}^\top\boldsymbol{G})\boldsymbol{n}_0|^2 \\ &\quad + \tfrac{1}{2}(k_2 + k_4)|\boldsymbol{F}^\top\boldsymbol{G}|^2 - \tfrac{1}{4}k_4\Big(\big(\operatorname{ax}(\boldsymbol{n}_0)\cdot(\boldsymbol{F}^\top\boldsymbol{G})\big)^2 + \big(\operatorname{ax}(\boldsymbol{F}^\top\boldsymbol{n})\cdot(\boldsymbol{F}^\top\boldsymbol{G})\big)^2\Big)\end{aligned} \tag{3.7}$$

of the Oseen–Zöcher–Frank energy density for uniaxial nematic elastomers with orientations $\boldsymbol{n}_0$ and $\boldsymbol{n}$ in the reference and deformed states (Anderson et al., 1999). The expression on the right-hand side of (3.6) is the nematic-elastomeric analogue of the *analyst's energy density*, [2] which, for nematic liquid-crystalline fluids, provides many qualitative and some quantitative insights. We refer to $\kappa > 0$ as the Frank modulus.

Summing (3.5) and (3.6) yields an expression,

$$\begin{aligned}\psi &= \widehat{\psi}(\boldsymbol{F},\boldsymbol{n},\boldsymbol{G}) \\ &= \frac{\mu}{2}\left(|\boldsymbol{F}|^2 - \frac{s-1}{s}|\boldsymbol{F}^\top\boldsymbol{n}|^2 + (s-1)|\boldsymbol{F}\boldsymbol{n}_0|^2 - \frac{(s-1)^2}{s}(\boldsymbol{F}^\top\boldsymbol{n}\cdot\boldsymbol{n}_0)^2 - 3\right) + \frac{\kappa(s-1)^2}{2s}|\boldsymbol{F}^\top\boldsymbol{G}|^2,\end{aligned} \tag{3.8}$$

for the total energy density $\psi = \psi_{\text{bulk}} + \psi_{\text{grad}}$ as a function $\widehat{\psi}$ of $\boldsymbol{F}$, $\boldsymbol{n}$, and $\boldsymbol{G}$.

On choosing the step-length anisotropy s equal to unity, (3.8) reduces to the conventional neo-Hookean energy density $\mu(|\boldsymbol{F}|^2 - 3)/2$. In this case, the step length is isotropic and the polymer molecules are random spherical coils. When s differs from unity, the molecules are ellipsoidal coils—oblate or prolate depending on whether s is less than or greater than unity, respectively.

4. Field equations

Bearing in mind the particular form (3.8) of the energy density, the deformational stress $\boldsymbol{S}$ is given (Anderson et al., 1999) by

$$\begin{aligned}\boldsymbol{S} &= \widehat{\boldsymbol{S}}(\boldsymbol{F},\boldsymbol{n},\boldsymbol{G}) - p\boldsymbol{F}^{-\top} \\ &= \mu\left(\boldsymbol{F} - \frac{s-1}{s}\boldsymbol{n}\otimes\boldsymbol{F}^\top\boldsymbol{n} + (s-1)\boldsymbol{F}\boldsymbol{n}_0\otimes\boldsymbol{n}_0 - \frac{(s-1)^2}{s}(\boldsymbol{F}^\top\boldsymbol{n}\cdot\boldsymbol{n}_0)\boldsymbol{n}\otimes\boldsymbol{n}_0\right) + \frac{\kappa(s-1)^2}{s}\boldsymbol{G}\boldsymbol{G}^\top\boldsymbol{F} - p\boldsymbol{F}^{-\top},\end{aligned} \tag{4.1}$$

with p a constitutively indeterminate pressure that reacts to the constraint $\det\boldsymbol{F} = 1$, while the internal orientational force $\boldsymbol{\pi}$ and the orientational stress $\boldsymbol{\Sigma}$ are given by [3]

$$\boldsymbol{\pi} = \widehat{\boldsymbol{\pi}}(\boldsymbol{F},\boldsymbol{n}) = \frac{\mu(s-1)}{s}(\boldsymbol{1} - \boldsymbol{n}\otimes\boldsymbol{n})\big(\boldsymbol{F}\boldsymbol{F}^\top + (s-1)\boldsymbol{F}\boldsymbol{n}_0\otimes\boldsymbol{F}\boldsymbol{n}_0\big)\boldsymbol{n} \tag{4.2}$$

[1] Here, $\operatorname{sym}\boldsymbol{A}$ denotes the symmetric component of the tensor $\boldsymbol{A}$ and $\operatorname{ax}(\boldsymbol{v})$ denote the axial tensor of $\boldsymbol{v}$, i.e., the unique skew tensor with the property that $(\operatorname{ax}(\boldsymbol{v}))\boldsymbol{u} = \boldsymbol{v}\times\boldsymbol{u}$ for all $\boldsymbol{u}$.

[2] What we call the analyst's energy density is also called *one-constant approximation* (Virga, 1994) and the *theoretician's energy* (*density*) (Stephen and Straley, 1974).

[3] As a consequence of the constraint $|\boldsymbol{n}| = 1$, the internal orientational force and the orientational stress generally include both active and reactive components. Anderson et al. (1999) consider both the active and reactive components of these fields and explain why determination of the multipliers that arise in response to the constraint $|\boldsymbol{n}| = 1$ are of negligible importance. Here, we therefore consider only the constitutively determinate (i.e., active) components of the internal orientational force and the orientational stress and denote these by $\boldsymbol{\pi}$ and $\boldsymbol{\Sigma}$.

and

$$\boldsymbol{\Sigma} = \widehat{\boldsymbol{\Sigma}}(\boldsymbol{F}, \boldsymbol{n}, \boldsymbol{G}) = \frac{\kappa(s-1)^2}{s}(\mathbf{1} - \boldsymbol{n} \otimes \boldsymbol{n})\boldsymbol{F}\boldsymbol{F}^{\top}\boldsymbol{G}, \tag{4.3}$$

respectively.

On neglecting external body forces and restricting attention to equilibrium, $\boldsymbol{S}$, $\boldsymbol{\Sigma}$, and $\boldsymbol{\pi}$ must comply with the field equations

$$\operatorname{Div}\boldsymbol{S} = \mathbf{0} \tag{4.4a}$$

and

$$\operatorname{Div}\boldsymbol{\Sigma} + (\boldsymbol{G} \cdot \boldsymbol{\Sigma})\boldsymbol{n} + \boldsymbol{\pi} = \mathbf{0}, \tag{4.4b}$$

expressing deformational and orientational-force balance. Moment balance, which requires that the tensor $\boldsymbol{S}\boldsymbol{F}^{\top} + \boldsymbol{n} \otimes \boldsymbol{\pi} + \boldsymbol{\Sigma}\boldsymbol{G}^{\top}$ be symmetric, is guaranteed provided that $\widehat{\psi}(\boldsymbol{Q}\boldsymbol{F}, \boldsymbol{Q}\boldsymbol{n}, \boldsymbol{Q}\boldsymbol{G}) = \widehat{\psi}(\boldsymbol{F}, \boldsymbol{n}, \boldsymbol{G})$ for all rotations $\boldsymbol{Q}$. A direct calculation shows that the particular choice (3.8) of $\widehat{\psi}$ possesses this invariance.

5. Nondimensionalization

Using δ to denote a characteristic length, we observe that μ, κ, and δ yield a single dimensionless parameter [4]

$$\epsilon = \frac{\kappa}{\mu\delta^2} > 0. \tag{5.1}$$

Labeling the unscaled fields with asterisks, we introduce the dimensionless independent and dependent variables

$$\boldsymbol{x} = \frac{\boldsymbol{x}^*}{\delta}, \quad \boldsymbol{y}(\boldsymbol{x}) = \frac{\boldsymbol{y}^*(\boldsymbol{x}^*)}{\delta}, \quad \boldsymbol{n}(\boldsymbol{x}) = \boldsymbol{n}^*(\boldsymbol{x}^*), \quad p(\boldsymbol{x}) = \frac{p^*(\boldsymbol{x}^*)}{\mu}, \tag{5.2}$$

and constitutive response functions

$$\left.\begin{aligned} &\widehat{\psi}(\boldsymbol{F}, \boldsymbol{n}, \boldsymbol{G}) = \frac{\widehat{\psi}^*(\boldsymbol{F}^*, \boldsymbol{n}^*, \boldsymbol{G}^*)}{\mu}, \quad \widehat{\boldsymbol{S}}(\boldsymbol{F}, \boldsymbol{n}, \boldsymbol{G}) = \frac{\widehat{\boldsymbol{S}}^*(\boldsymbol{F}^*, \boldsymbol{n}^*, \boldsymbol{G}^*)}{\mu}, \\ &\widehat{\boldsymbol{\pi}}(\boldsymbol{F}, \boldsymbol{n}) = \frac{\widehat{\boldsymbol{\pi}}^*(\boldsymbol{F}^*, \boldsymbol{n}^*)}{\mu}, \quad \widehat{\boldsymbol{\Sigma}}(\boldsymbol{F}, \boldsymbol{n}, \boldsymbol{G}) = \frac{\widehat{\boldsymbol{\Sigma}}^*(\boldsymbol{F}^*, \boldsymbol{n}^*, \boldsymbol{G}^*)}{\mu\delta}. \end{aligned}\right\} \tag{5.3}$$

From (3.8), (4.1)–(4.3), (5.2), and (5.3) it follows that

$$\psi = \frac{1}{2}\left(|\boldsymbol{F}|^2 - \frac{s-1}{s}|\boldsymbol{F}^{\top}\boldsymbol{n}|^2 + (s-1)|\boldsymbol{F}\boldsymbol{n}_0|^2 - \frac{(s-1)^2}{s}(\boldsymbol{F}^{\top}\boldsymbol{n} \cdot \boldsymbol{n}_0)^2 - 3\right) + \frac{\epsilon(s-1)^2}{2s}|\boldsymbol{F}^{\top}\boldsymbol{G}|^2, \tag{5.4a}$$

$$\boldsymbol{S} = \boldsymbol{F} - \frac{s-1}{s}\boldsymbol{n} \otimes \boldsymbol{F}^{\top}\boldsymbol{n} + (s-1)\boldsymbol{F}\boldsymbol{n}_0 \otimes \boldsymbol{n}_0 - \frac{(s-1)^2}{s}(\boldsymbol{F}^{\top}\boldsymbol{n} \cdot \boldsymbol{n}_0)\boldsymbol{n} \otimes \boldsymbol{n}_0 + \frac{\epsilon(s-1)^2}{s}\boldsymbol{G}\boldsymbol{G}^{\top}\boldsymbol{F} - p\boldsymbol{F}^{-\top}, \tag{5.4b}$$

[4] If we take $\delta \sim 10^{-5}$ m, which is of the order of the characteristic stripe width observed in the experiment of Kundler and Finkelmann (1995), and, following Verwey et al. (1996), assume that $\mu \sim 10^5$ N/m^2 and that $\kappa \sim 10^{-11}$ N, (5.1) yields $\epsilon = 10^{-6}$.

$$\pi = \frac{(s-1)}{s}(\mathbf{1} - \boldsymbol{n}\otimes\boldsymbol{n})\big(\boldsymbol{F}\boldsymbol{F}^{\top} + (s-1)\boldsymbol{F}\boldsymbol{n}_0 \otimes \boldsymbol{F}\boldsymbol{n}_0\big)\boldsymbol{n}, \tag{5.4c}$$

$$\boldsymbol{\Sigma} = \frac{\epsilon(s-1)^2}{s}(\mathbf{1} - \boldsymbol{n}\otimes\boldsymbol{n})\boldsymbol{F}\boldsymbol{F}^{\top}\boldsymbol{G}. \tag{5.4d}$$

Henceforth, we write $\mathscr{R}$ for the region associated with the dimensionless position $\boldsymbol{x}$, use grad and div to denote the gradient and divergence on $\mathscr{R}$, and work only with dimensionless quantities. The field equations are then (4.4a) and (4.4b) with $\boldsymbol{S}$, π, and $\boldsymbol{\Sigma}$ as given in (5.4a)–(5.4d).

6. Specimen geometry: kinematic assumptions

Referring to the experiment of Kundler and Finkelmann (1995), we select a right-handed Cartesian basis $\{\boldsymbol{e}_1, \boldsymbol{e}_2, \boldsymbol{e}_3\}$, with $\boldsymbol{e}_1$ parallel to the axis of loading and $\boldsymbol{e}_2 = \boldsymbol{n}_0$, and suppose that the region $\mathscr{R}$ occupied by the body in the undeformed reference state has the form

$$\mathscr{R} = \{\boldsymbol{x} : 0 < \boldsymbol{x}\cdot\boldsymbol{e}_1 < l_1, \quad 0 < \boldsymbol{x}\cdot\boldsymbol{e}_2 < l, \quad 0 < \boldsymbol{x}\cdot\boldsymbol{e}_3 < l_3\} \tag{6.1}$$

of a rectangular sheet. We write $x = \boldsymbol{x}\cdot\boldsymbol{e}_2$ for the coordinate that lies in-plane and is perpendicular to the axis of loading.

Following Verwey et al. (1996), we assume that

$$\boldsymbol{F} = f\boldsymbol{e}_1\otimes\boldsymbol{e}_1 + \frac{1}{f}\boldsymbol{e}_2\otimes\boldsymbol{e}_2 + \boldsymbol{e}_3\otimes\boldsymbol{e}_3 + \gamma\boldsymbol{e}_1\otimes\boldsymbol{e}_2, \tag{6.2}$$

which corresponds to a plane strain with uniform stretch f along the axis of loading and in-plane shear γ possibly dependent on x, and that

$$\boldsymbol{n} = (\sin\varphi)\boldsymbol{e}_1 + (\cos\varphi)\boldsymbol{e}_2, \tag{6.3}$$

which corresponds to a unit vector field in the plane of the undeformed specimen, with φ possibly dependent on x and taking values between $-\pi/2$ and $\pi/2$. [5]

On using (6.2) and (6.3) in 5.4a and bearing in mind that $\boldsymbol{n}_0 = \boldsymbol{e}_2$, it follows that

$$\psi = \frac{(f^2-1)^2}{2f^2} + \widetilde{\psi}(\gamma,\varphi,\varphi'), \tag{6.4}$$

where a superposed prime denotes differentiation with respect to x and

$$\begin{aligned}\widetilde{\psi}(\gamma,\varphi,\varphi') = {}& \frac{\gamma^2}{2} - \frac{s-1}{2}\left(\frac{f^2\sin^2\varphi}{s} - \left(\gamma\cos\varphi - \frac{\sin\varphi}{f}\right)^2\right)\\ & + \frac{\epsilon(s-1)^2}{2s}\left(f^2\cos^2\varphi + \left(\gamma\cos\varphi - \frac{\sin\varphi}{f}\right)^2\right)|\varphi'|^2.\end{aligned} \tag{6.5}$$

As for $\boldsymbol{S}$, π, and $\boldsymbol{\Sigma}$, a calculation analogous to that leading to (6.4) and (6.5) yields [6]

$$\boldsymbol{S} = S_{\alpha\beta}\boldsymbol{e}_\alpha\otimes\boldsymbol{e}_\beta + S_{33}\boldsymbol{e}_3\otimes\boldsymbol{e}_3, \tag{6.6a}$$

[5] Due to considerations of material symmetry (Anderson et al., 1999), we do not distinguish between $\boldsymbol{n}$ and $-\boldsymbol{n}$.

[6] We employ the summation convention, with the indices α and β running over $\{1,2\}$.

$$\boldsymbol{\pi} = \pi_\alpha \boldsymbol{e}_\alpha, \tag{6.6b}$$

and

$$\boldsymbol{\Sigma} = \Sigma_{\alpha 2} \boldsymbol{e}_\alpha \otimes \boldsymbol{e}_2, \tag{6.6c}$$

with

$$S_{11} = \frac{f}{s} + \frac{f(s-1)\cos^2\varphi\left(1+\epsilon(s-1)|\varphi'|^2\right)}{s} - \frac{p}{f}, \tag{6.7a}$$

$$S_{12} = \gamma + \frac{(s-1)\cos\varphi(f\gamma\cos\varphi - \sin\varphi)\left(s+\epsilon(s-1)|\varphi'|^2\right)}{sf}, \tag{6.7b}$$

$$S_{21} = -\frac{(s-1)f\sin\varphi\cos\varphi\left(1+\epsilon(s-1)|\varphi'|^2\right)}{s} + p\gamma, \tag{6.7c}$$

$$S_{22} = \frac{1}{f} - \frac{(s-1)\sin\varphi(f\gamma\cos\varphi - \sin\varphi)\left(s+\epsilon(s-1)|\varphi'|^2\right)}{sf} - pf, \tag{6.7d}$$

$$S_{33} = 1 - p, \tag{6.7e}$$

and

$$\pi_1 = \frac{(s-1)\cos\varphi}{s}\left(\frac{s\gamma\cos 2\varphi}{f} + \left(f^2 + s\gamma^2 - \frac{s}{f^2}\right)\sin\varphi\cos\varphi\right), \tag{6.8a}$$

$$\pi_2 = -\frac{(s-1)\sin\varphi}{s}\left(\frac{s\gamma\cos 2\varphi}{f} + \left(f^2 + s\gamma^2 - \frac{s}{f^2}\right)\sin\varphi\cos\varphi\right), \tag{6.8b}$$

$$\Sigma_{12} = \frac{\epsilon(s-1)^2\cos\varphi}{s}\left((f^2+\gamma^2)\cos^2\varphi - \frac{2\gamma}{f}\sin\varphi\cos\varphi + \frac{\sin^2\varphi}{f^2}\right)\varphi', \tag{6.8c}$$

$$\Sigma_{22} = -\frac{\epsilon(s-1)^2\sin\varphi}{s}\left((f^2+\gamma^2)\cos^2\varphi - \frac{2\gamma}{f}\sin\varphi\cos\varphi + \frac{\sin^2\varphi}{f^2}\right)\varphi'. \tag{6.8d}$$

Granted that γ and φ vary at most with x, (6.5), (6.6b), (6.6c), and (6.8a)–(6.8d) imply that ψ, $\boldsymbol{\Sigma}$, and $\boldsymbol{\pi}$ also depend only on x. Similarly, unless p is found to depend on coordinates other than x, (6.6a) and (6.7a)–(6.7e) imply that $\boldsymbol{S}$ depends at most on x.

7. Boundary conditions

We require that the surfaces of the specimen with unit normal $\boldsymbol{e}_2$ be free of deformational traction, viz., [7]

$$\boldsymbol{S}(0)\boldsymbol{e}_2 = \boldsymbol{S}(l)\boldsymbol{e}_2 = \boldsymbol{0}, \tag{7.1}$$

but allow for nontrivial deformational tractions on the remaining surfaces of the specimen.

[7] Here, for simplicity, we suppress possible dependence of $\boldsymbol{S}$ on coordinates other than x.

In addition, we require that the orientational traction on the surfaces of the specimen with unit normal $\boldsymbol{e}_2$ be free of orientational traction, viz.,

$$\boldsymbol{\Sigma}(0)\boldsymbol{e}_2 = \boldsymbol{\Sigma}(l)\boldsymbol{e}_2 = \boldsymbol{0}. \tag{7.2}$$

From (6.8a)–(6.8d), it follows that the orientational tractions on the faces of the remaining surfaces of the specimen vanish.

8. Boundary-value problem

The deformational force balance (4.4a) together with the boundary conditions (7.1) require that $S_{12} = S_{22} = 0$. Using (6.7b) and (6.7d), we therefore obtain the relations,

$$\gamma = \frac{(s-1)(\sin\varphi\cos\varphi)\left(s + \epsilon(s-1)|\varphi'|^2\right)}{f\left(s\sin^2\varphi + s^2\cos^2\varphi + \epsilon(s-1)^2(\cos^2\varphi)|\varphi'|^2\right)} \tag{8.1}$$

and

$$p = \frac{s^2 + \epsilon(s-1)^2|\varphi'|^2}{f^2\left(s\sin^2\varphi + s^2\cos^2\varphi + \epsilon(s-1)^2(\cos^2\varphi)|\varphi'|^2\right)}, \tag{8.2}$$

determining γ and p in terms of φ and φ'. Using these in (6.7a), (6.7c) and (6.7e) yields expressions for S_{11}, S_{21}, and S_{33} in terms of φ and φ'. From (8.2), it follows that $\boldsymbol{S}$ varies only with x. [8]

The orientational-force balance (4.4b) reduces to a single scalar ordinary differential equation, which can be expressed concisely as

$$\left(\frac{\partial\widetilde{\psi}(\gamma,\varphi,\varphi')}{\partial\varphi'}\right)' = \frac{\partial\widetilde{\psi}(\gamma,\varphi,\varphi')}{\partial\varphi}. \tag{8.3}$$

In view of (8.1) and (8.3) is a second-order ordinary-differential-equation for φ. Boundary conditions for φ follow from (6.8c) and (6.8d) and (7.2), which requires that

$$\varphi'(0) = \varphi'(l) = 0. \tag{8.4}$$

9. Solutions of the boundary-value problem

9.1. Homogeneous solutions

Homogeneous solutions of the boundary-value problem (8.3) and (8.4) are determined by the equation

$$\frac{\partial\widetilde{\psi}(\gamma,\varphi,0)}{\partial\varphi} = \left(\frac{f^2}{s} - \frac{s^2}{f^2(\sin^2\varphi + s\cos^2\varphi)^2}\right)\sin\varphi\cos\varphi = 0, \tag{9.1}$$

[8] In general, S_{11}, S_{21}, and S_{33} are nonvanishing. However, if we interpret the kinematical Ansatz (6.2) as an internal constraint and introduce a reactive stress that responds to this constraint, this stress cancels S_{11}, S_{21}, and S_{33}, rendering the equilibrium state stress-free.

which yields

$$\varphi = 0, \quad \varphi = \pm\frac{\pi}{2}, \tag{9.2a}$$

$$\varphi = \pm \arcsin\left(\frac{1}{f}\sqrt{\frac{s(f^2-1)}{s-1}}\right). \tag{9.2b}$$

Shears,

$$\gamma = 0, \quad \gamma = 0, \tag{9.3a}$$

$$\gamma = \pm\frac{1}{f}\sqrt{\frac{(f^2-1)(s-f^2)}{s}}, \tag{9.3b}$$

corresponding to the homogeneous solutions (9.2a) and (9.2b) of (8.3) and (8.4) are determined on using (9.2a) and (9.2b) in (8.1).

The relations (9.2b) and (9.3b) are valid if $0 < s < 1$ and $\sqrt{s} < f < 1$, which coincides with stretching a specimen with oblate backbone anisotropy along the $\boldsymbol{e}_2$-axis, or if $s > 1$ and $1 < f < \sqrt{s}$, which coincides with stretching a specimen with prolate backbone anisotropy along the $\boldsymbol{e}_1$-axis. Motivated by the experiments performed by Kundler and Finkelmann (1995), Talroze et al. (1999) and Zubarev et al. (1999), we assume hereafter that

$$s > 1 \tag{9.4a}$$

and

$$1 < f < \sqrt{s}. \tag{9.4b}$$

9.2. Inhomogeneous solutions

The homogeneous solutions (9.2a) and (9.2b) correspond to fixed points of the differential Eq. (8.3). An eigenvalue analysis reveals that, of these, only the elliptic point (9.2a) may bifurcate into inhomogeneous solutions. Guided by the experiment of Kundler and Finkelmann (1995), where the undistorted state of the nematic elastomer corresponds to the trivial solution $\varphi = 0$, we focus attention on bifurcations that emanate from this point.

Linearizing (8.3) about $\varphi = 0$ and seeking solutions consistent with the boundary conditions (8.4), we find that bifurcations from $\varphi = 0$ may occur for critical values

$$f_n = \frac{\sqrt{l}}{(l^2 - \epsilon(s-1)n^2\pi^2)^{1/4}}, \tag{9.5}$$

of the stretch f, where, by (9.4a) and (9.4b), the positive integer n obeys the inequality

$$n < \frac{l\sqrt{1+s}}{\sqrt{\epsilon}\pi s}. \tag{9.6}$$

Inhomogeneous solutions of (8.3) and (8.4) can then be constructed using the first integral

$$\varphi' \frac{\partial \widetilde{\psi}(\gamma, \varphi, \varphi')}{\partial \varphi'} = \widetilde{\psi}(\gamma, \varphi, \varphi') + \text{constant} \tag{9.7}$$

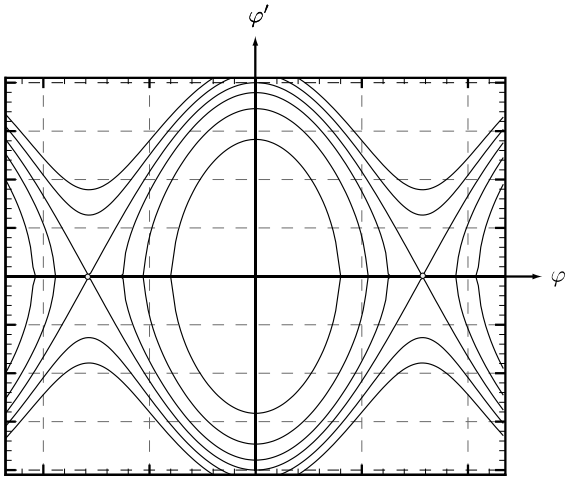

Fig. 1. Schematic of the phase portrait for the Eq. (8.3). Due to the range $[-\pi/2, \pi/2]$ of φ, it is useful to think of the phase portrait as lying on the surface of a circular cylinder with axis along φ'. Elliptic points occur at $\varphi = 0$ and $\varphi = \pi/2$ (or, equivalently, $\varphi = -\pi/2$) and the hyperbolic points $\varphi = \pm \arcsin((1/f)(s(f^2-1)/(s-1))^{1/2})$ are connected by two heteroclinic orbits.

of (8.3). Specifically, as the first integral is constant along any solution of (8.3), all the solutions of the boundary-value problem correspond to level sets of (9.7) (see Fig. 1). Due to the Neumann boundary conditions (8.4), these solutions must begin and terminate on the φ-axis of the phase portrait. Using the well-established argument involving the specimen's finite width l (see, for example, Cusumano et al., 1998), we conclude that only a finite number of such orbits serve as inhomogeneous solutions. Corresponding to an orbit that does exactly n half-turns about the central trivial solution there therefore exist periodic solutions

$$\varphi_n(x) = \pm a_n \cos\left(\frac{n\pi x}{l}\right) \tag{9.8}$$

describing a pair of states involving $n+1$ stripes separated by n transition layers. Across each such layer, the orientation and shear vary between the homogeneous values (9.2b) and (9.3b).

10. Local stability of inhomogeneous solutions

To obtain information concerning the local stability of the inhomogeneous solutions discussed above, we study the cubic approximation

$$\epsilon(s-1)\left(1+\frac{1-s^2f^4}{s^2f^4}\varphi^2\right)\varphi'' + \epsilon(s-1)\left(\frac{1-s^2f^4}{s^2f^4}\right)|\varphi'|^2\varphi + \left(1-\frac{1}{f^4}\right)\varphi - \frac{2}{f^4}\left(\frac{s-1}{s}+\frac{f^4-1}{3}\right)\varphi^3 = 0 \tag{10.1}$$

of (8.3), which resembles the Euler equation of column buckling.

Introducing the local stretch parameter

$$\alpha_n = f - f_n, \tag{10.2}$$

we apply the Lyapunov–Schmidt method to (10.1) and obtain the bifurcation function

$$g(a_n,\alpha_n)=\frac{4f_n a_n\alpha_n(l^2-\epsilon(s-1)n^2\pi^2)}{sl^2}-\frac{s^2(f_n^4-1)l^2+3s(s-1)l^2+\epsilon(s-1)(1-s^2f_n^4)n^2\pi^2}{2s^3f_n^2l^2}a_n^3+o(a_n^3), \tag{10.3}$$

with a_n the amplitude of the solution. On setting $g(a_n,\alpha_n)=0$, we arrive at

$$\alpha_n=\frac{s^2(f_n^4-1)l^2+3s(s-1)l^2+\epsilon(s-1)(1-s^2f_n^4)n^2\pi^2}{8s^2f_n^3(l^2-\epsilon(s-1)n^2\pi^2)}a_n^2+o(a_n^2). \tag{10.4}$$

A solution is locally stable or unstable depending on whether the derivative

$$\frac{\partial g(a_n,\alpha_n)}{\partial a_n}=\frac{4f_n\alpha_n(l^2-\epsilon(s-1)n^2\pi^2)}{sl^2}-\frac{3s^2(f_n^4-1)l^2+9s(s-1)l^2+3\epsilon(s-1)(1-s^2f_n^4)n^2\pi^2}{2s^3f_n^2l^2}a_n^2+o(a_n^2) \tag{10.5}$$

is negative or positive (Golubitsky and Schaeffer, 1985). For the trivial solution, which corresponds to the choice $a_n=0$, we have

$$\left.\frac{\partial g(a_n,\alpha_n)}{\partial a_n}\right|_{a_n=0}=\frac{4f_n\alpha_n(l^2-\epsilon(s-1)n^2\pi^2)}{sl^2}. \tag{10.6}$$

Hence, the trivial solution is stable or unstable depending on whether a_n is negative or positive, respectively. Further, granted (10.4),

$$\frac{\partial g(a_n,\alpha_n)}{\partial a_n}=-\frac{s^2(f_n^4-1)l^2+3s(s-1)l^2+\epsilon(s-1)(1-s^2f_n^4)n^2\pi^2}{s^3f_n^2l^2}a_n^2, \tag{10.7}$$

and it follows that, once it comes into existence, the nontrivial solution corresponding to (10.4) is locally stable. This is a classical exchange of stability: to the left of the bifurcation point, only the trivial solution is stable, whereas, to the right of the bifurcation point, stability is transferred to the nontrivial solution.

11. Thickness of the interstripe layer

Considering a state involving $n+1$ stripes, we assume that the n transition layers connecting these stripes have identical thickness. We describe a generic interstripe layer as a set

$$\left\{x:|\varphi'(x)|>\xi\max_{0<x<l}|\varphi'|\right\}, \tag{11.1}$$

with ξ belonging to $(0,1)$ a dimensionless cut-off constant to be chosen, and write $\pm\varphi_n^*$ for the values of φ at the limits of the layer.

Following Fried and Grach (1997), we use the first integral (9.7) to develop an analytical estimate for the thickness ℓ_n of an interstripe layer. We assume that the stretch f is close to a bifurcation point f_n, so that (9.8) yields a valid approximation for φ. Consistent with the scaling introduced in Section 5, we assume also that $\sqrt{\epsilon}\varphi'$ is of the same order of magnitude as φ. Then, expanding (9.7) up to the third order in φ, we obtain

$$\epsilon(s-1)|\varphi'|^2=\left(1-\frac{1}{f^4}\right)(a_n^2-\varphi^2), \tag{11.2}$$

which, upon separating variables, integrating over the layer and simplification, yields

$$\ell_n = \frac{2\sqrt{\epsilon(s-1)}f^2}{\sqrt{f^4-1}} \arcsin\left(\frac{\varphi_n^*}{a_n}\right). \tag{11.3}$$

From (11.2), it follows that

$$\max_{0<x<l}|\varphi'| = \sqrt{\frac{1}{\epsilon(s-1)}\left(1-\frac{1}{f^4}\right)}a_n. \tag{11.4}$$

Invoking the definition (11.1) of the layer and using (11.4) in (11.2) then yields

$$\varphi_n^* = \sqrt{1-\xi^2}a_n. \tag{11.5}$$

Thus, by (11.3), the interstripe thickness is independent of the number of stripes and, writing

$$\ell = \ell_n, \tag{11.6}$$

we obtain the estimate

$$\ell = \frac{2\sqrt{\epsilon(s-1)}f^2 \arcsin\sqrt{1-\xi^2}}{\sqrt{f^4-1}}. \tag{11.7}$$

The lack of n-dependence in this estimate shows that the localization processes which gives rise to an interstripe layer is insensitive to the material state in the far field. On the other hand, the thickness of the layer shows tangible dependence upon the axial stretch f. This dependence stems from the factor of $\boldsymbol{F}^\top$ present in the gradient-energy density (3.6), a factor which gives rise to dependencies upon f and γ in the coefficient of $|\varphi'|^2$ in (6.5) and which is required (Anderson et al., 1999) to ensure invariance.

12. Energy of the interstripe layer

We now consider the problem of estimating the energy of a transition layer in a state involving $n+1$ stripes. We consider a generic interstripe layer centered at a point x_* and, accounting for the uniform elastic contribution arising from the first term on the right-hand side of (6.4), define the energy $\mathscr{E}_n$ of the layer by

$$\mathscr{E}_n = \int_{x_*-\frac{\ell}{2}}^{x_*+\frac{\ell}{2}} \left(\frac{(f^2-1)^2}{2f^2} + \widetilde{\psi}(\gamma,\varphi,\varphi')\right) \mathrm{d}x. \tag{12.1}$$

Taking for γ the expression (8.1), we expand $\widetilde{\psi}$ up to the third order in φ and employ (11.2). This yields an approximation of $\widetilde{\psi}$ in terms of φ. Inserting this expression in (12.1), we obtain

$$\begin{aligned}\mathscr{E}_n = {} & \frac{(f^2-1)^2\ell}{2f^2} + \frac{(s-1)(f^4-1)a_n^2\ell}{2sf^2} + \frac{1}{2}\left(\frac{f^4-(f^4-1)(2s+(s-1)a_n^2-1)}{sf^2}\right. \\ & \left. - \frac{sf^2}{s^2f^4+(s-1)(f^4-1)a_n^2}\right)\int_{x_*-\frac{\ell}{2}}^{x_*+\frac{\ell}{2}} \varphi^2 \,\mathrm{d}x.\end{aligned} \tag{12.2}$$

To evaluate the integral on the right-hand side of (12.2), we use (11.2) to make a change of variables and find that

$$\int_{x_*-\frac{\ell}{2}}^{x_*+\frac{\ell}{2}} \varphi^2 \,\mathrm{d}x = \frac{\sqrt{\epsilon(s-1)}f^2\left(\arcsin\sqrt{1-\xi^2}-\xi\sqrt{1-\xi^2}\right)a_n^2}{\sqrt{f^4-1}}. \tag{12.3}$$

Thus, combining (12.2) with (12.3) and using (11.7), we determine an estimate

$$\mathscr{E}_n = \sqrt{\epsilon(s-1)}\left(\frac{(f^2-1)\arcsin\sqrt{1-\xi^2}}{\sqrt{f^2+1}} + \mathscr{A}_n(f,s,\xi)\right), \tag{12.4}$$

with

$$\mathscr{A}_n(f,s,\xi) = \left(\frac{(s-1)\sqrt{f^4-1}\xi\sqrt{1-\xi^2}}{s} + \left(\frac{1-(s-1)(f^4-1)a_n^2}{2s\sqrt{f^4-1}} - \frac{sf^2}{s^2f^4+(s-1)(f^4-1)a_n^2}\right) \times \left(\arcsin\sqrt{1-\xi^2}-\xi\sqrt{1-\xi^2}\right)\right)a_n^2, \tag{12.5}$$

for the energy of the layer. Unlike (11.7) and (12.4) depends upon the number n of interstripe layers present through the amplitude a_n.

13. Numerical results

13.1. Solution of the boundary-value problem (8.3) and (8.4)

To illustrate the foregoing ideas, we take

$$\epsilon = 10^{-6}, \tag{13.1}$$

which corresponds to setting the characteristic length δ equal to the stripe width 10^{-5} m observed by Kundler and Finkelmann (1995) and chosing the shear modulus μ and the Frank modulus κ equal to 10^5 N/m^2 and 10^{-11} N, respectively. Further, we take

$$s = 2, \tag{13.2}$$

which corresponds to the step-length anisotropy present in the specimens of Kundler and Finkelmann (1995). By (9.4b), the choice (13.2) requires that the axial stretch f obey

$$1 < f < \sqrt{2}. \tag{13.3}$$

For simplicity, we assume that

$$l = 1 \tag{13.4}$$

and confine attention to solutions involving a single stripe, so that

$$n = 1. \tag{13.5}$$

Granted these choices, we solve the boundary-value problem (8.3) and (8.4) numerically for 414 equally spaced values of f ranging between 1 and 1.414. To do so, we replace (8.3) by a parabolic partial differential equation

$$\beta\dot{\varphi} = \left(\frac{\partial\widetilde{\psi}(\gamma,\varphi,\varphi')}{\partial\varphi'}\right)' - \frac{\partial\widetilde{\psi}(\gamma,\varphi,\varphi')}{\partial\varphi}, \tag{13.6}$$

where a prime denotes partial differentiation with respect to space, a superposed dot denotes partial differentiation with respect to (dimensionless) time, and $\beta > 0$ is a (dimensionless) *dissipation coefficient*. For β, we choose

$$\beta = 0.1. \tag{13.7}$$

To discretize (13.6), we employ an implicit finite difference scheme which approximates first derivatives in space and time and second derivatives in space by central differences. For the spatial mesh, we generate an spatially inhomogeneous grid x_i, $i = 1,\ldots,n$, with $n = 2000$ nodes according to the formula

$$x_i = \frac{\xi_i + 10000(1 + (2\xi_i - 1)^5)}{20001}, \tag{13.8}$$

with ξ_i, $i = 1,\ldots,n$, distributed equidistantly in the interval [0,1] (for details, see, e.g., Knupp and Steinberg (1993)). This grid makes it possible to zoom in on the region about $x = 0.5$ where we find that the orientation undergoes an abrupt change. To deal with the nonlinearities present in (13.6), we simply employ Newton's method.

At the boundaries, we continue to impose the Newmann conditions (8.4).

Initially, we choose an intermediate value of stretch, take initial conditions resembling a step function (with jump located at $x = 0.5$) and march forward in time, with step $\Delta t = 1$. This process is continued until the solution converges in time. We then increment the stretch, using as initial condition the solution obtained at previous step.

To formulate the convergence criteria, we define the norm

$$\|\varphi\| = \left(\sum_{i=0}^{n} \varphi^2(x_i)\right)^{1/2}, \tag{13.9}$$

and say that the process converges if the norm (13.9) of the increment is less than some tolerance. For tolerances, we choose: for Newton's method, $\mathrm{tol}_{\mathrm{N}} = 10^{-8}$; and, for time stepping, $\mathrm{tol} = 10^{-5}$.

To test convergence with respect to spatial space-size, we compute the solutions for stretches starting from $f = 1.1$ and ending at $f = 1.9$ with the step of 0.1 with $n = 1000$, $n = 2000$, and $n = 4000$ and observe that with increasing n the norm of the difference between those solutions steadily decreases, thus leading to convergence. Fig. 2 shows plots of the orientation and shear obtained for $f = 1.3$.

13.2. Thickness of the interstripe layer

With these numerically obtained solutions in place, we invoke the definition (11.1) with $\xi = 9/10$ to compute the thickness ℓ_1 of the interstripe layer for each value of f. Fig. 3 compares the numerically determined thicknesses with the predictions of the estimate (11.7) specialized to the case $n = 1$. At the first bifurcation point, the layer is of considerable thickness. With increasing stretch, the layer thins and reaches a minimum near $f = 1.25$. The layer then thickens and reaches a limiting value at $f = 1.414$. Fig. 3 shows that the asymptotic result (11.7) gives a remarkably good estimate of the layer thickness. However, the estimate decreases monotonically with f and, thus, fails to capture the local maximum exhibited by the numerical solution.

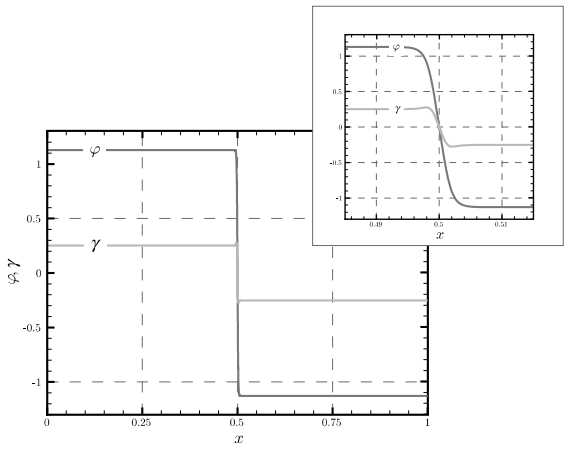

Fig. 2. Plots of φ and γ for an inhomogeneous equilibrium solution with a single interstripe layer, computed for $\epsilon = 10^{-6}$, $l = 1$, $s = 2$, and $f = 1.3$. The layer is resolved in the subplot.

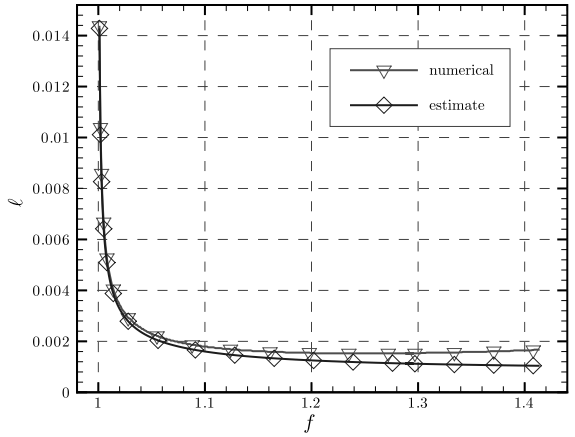

Fig. 3. Thickness ℓ of the interstripe wall versus stretch f, computed in accordance with the definition (11.1), for $\epsilon = 10^{-6}$, $s = 2$, $n = 1$, and $\xi = 9/10$ and compared to the predictions of the theoretical estimate (11.7) for $l = 1$, $n = 1$.

13.3. Energy of the interstripe layer

Using, once again, the numerically generated solutions and the definition (11.1) with $\xi = 9/10$, we compute the energy $\mathscr{E}_1$ of the interstripe layer using the trapezoidal rule. Fig. 4 compares the numerically determined energy with the predictions of estimate (12.4) specialized to the case $n = 1$. Both approaches indicate that $\mathscr{E}_1$ grows monotonically with f. As with the estimate for the thickness of the interstripe layer, the estimate (12.4) gives a remarkably good estimate of the energy of the interstripe layer. However, whereas (11.7) underestimates the thickness of the layer, (12.4) overestimates the energy of the layer.

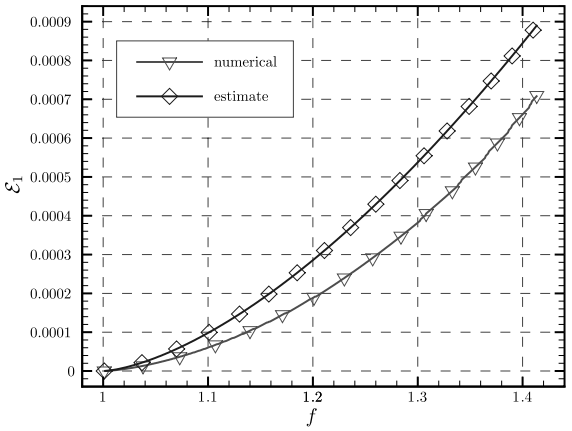

Fig. 4. Free energy $\mathscr{E}_1$ of the interstripe layer versus stretch f, computed in accordance with the definition (11.1), for $\epsilon = 10^{-6}$, $s = 2$, and $\xi = 9/10$ and compared to the predictions of the theoretical estimate (12.4) for $l = 1$, $n = 1$.

14. Conclusions

Our results explain stripe formation in a clamped and uniaxially extended nematic-elastomeric sheet as a bifurcation that occurs due to the need to accommodate extension while prohibiting macroscopic shear. We obtain analytical estimates of the thickness and energy of interstripe layers and a comparison with numerical results obtained for a solution involving a single interstripe layer shows these estimates to be quite reliable over the entire interval of axial stretches. Nevertheless, the one-dimensional nature of our problem makes it impossible to predict the number of stripes present in a specimen of given thickness and, hence, the thickness of individual stripes. The obstacles encountered in attempting to extend our approach to deal with more than one spatial dimension are primarily of a numerical character. Currently a finite-element formulation for the two-dimensional case is underway.

Acknowledgements

We thank the National Science Foundation for support under grant CMS 96-10286.

References

Anderson, D.R., Carlson, D.E., Fried, E., 1999. A continuum mechanical theory for nematic elastomers. Journal of Elasticity 56, 33–58.

Cusumano, J.P., Sikora, J., Jester, W., 1998. Spatially periodic solutions in a 1D model of phase transitions with order parameter. Physica D 121, 275–294.

Fridrikh, S.V., Terentjev, E.M., 1999. Polydomain-monodomain transition in nematic elastomers. Physical Review E 60, 1847–1857.

Fried, E., Grach, G., 1997. An order parameter-based theory as a regularization of a sharp interface theory for solid–solid phase transitions. Archive for Rational Mechanics and Analysis 138, 355–404.

Golubitsky, M., Schaeffer, D.G., 1985. Singularities and Groups in Bifurcation Theory, vol. 1. Springer-Verlag, New York.

Knupp, P.M., Steinberg, S., 1993. The Fundamentals of Grid Generation. CRC Press, Boca Raton.

Kundler, I., Finkelmann, H., 1995. Strain-induced director reorientation in nematic liquid single crystal elastomers. Macromolecular Rapid Communications 16, 679–686.

Roberts, P.M.S., Mitchell, G.R., Davis, F.J., 1997. A single director switching mode for monodomain liquid crystal elastomers. Journal de Physique II 7, 1337–1351.

Stephen, M.J., Straley, J.P., 1974. Physics of liquid crystals. Reviews of Modern Physics 46, 617–704.

Talroze, R.V., Zubarev, E.R., Kuptsov, S.A., Merekalov, A.S., Yuranova, T.I., Plate, N.A., Finkelmann, H., 1999. Liquid crystal acrylate-based networks: polymer backbone-LC order interaction. Reactive & Functional Polymers 41, 1–11.

Verwey, G.C., Warner, M., Terentjev, E.M., 1996. Elastic instability and stripe domains in liquid crystalline elastomers. Journal de Physique II 6, 1273–1290.

Virga, E.G., 1994. Variational Theories for Liquid Crystals. Chapman and Hall, London.

Warner, M., Gelling, K.P., Vilgis, T.A., 1988. Theory of nematic networks. Journal of Chemical Physics 88, 4008–4013.

Zubarev, E.R., Kuptsov, S.A., Yuranova, T.I., Talroze, R.V., Finkelmann, H., 1999. Monodomain liquid crystalline networks: reorientation mechanism from uniform to stripe domains. Liquid Crystals 26, 1531–1540.